

The galaxy luminosity function around groups.

González, R. E., Padilla, N.D., Galaz, G., & Infante, L.

Departamento de Astronomía y Astrofísica, Pontificia Universidad Católica de Chile, V. Mackenna 4860, Santiago 22, Chile.

8 September 2018

ABSTRACT

We present a study on the variations of the luminosity function of galaxies around clusters in a numerical simulation with semi-analytic galaxies, attempting to detect these variations in the 2dF Galaxy Redshift Survey. We subdivide the simulation box in equal-density regions around clusters, which we assume can be achieved by selecting objects at a given normalised distance (r/r_{rms} , where r_{rms} is an estimate of the halo radius) from the group centre. The semi-analytic model predicts important variations in the luminosity function out to $r/r_{rms} \simeq 5$. In brief, variations in the mass function of haloes around clusters (large dark-matter haloes with $M > 10^{12}h^{-1}M_{\odot}$) lead to cluster central regions that present a high abundance of bright galaxies (high M^* values) as well as low luminosity galaxies (high α); at $r/r_{rms} \simeq 3$ there is a lack of bright galaxies, which shows the depletion of galaxies in the regions surrounding clusters (minimum in M^* and α), and a tendency to constant luminosity function parameters at larger cluster-centric distances. We take into account the observational biases present in the real data by reproducing the peculiar velocity effect on the redshifts of galaxies in the simulation box, and also by producing mock catalogues. We find that excluding from the analysis galaxies which in projection are close to the centres of the groups provides results that are qualitatively consistent with the full simulation box results. When we apply this method to mock catalogues of the 2dF Galaxy Redshift Survey (2dFGRS) and the 2PIGG catalogue of groups, we find that the variations in the luminosity function are almost completely erased by the finger-of-god effect; only a lack of bright galaxies at $r/r_{rms} \simeq 3$ can be marginally detected in the mock catalogues. The results from the real 2dFGRS data shows a more clear detection of a dip in M^* and α for $r/r_{rms} = 3$, consistent with the semi-analytic predictions.

Key words: large-scale structure of the universe, methods: N-body simulations, galaxies: kinematics and dynamics cosmology: theory

1 INTRODUCTION

Understanding the way in which galaxies form is a key challenge facing cosmologists today. This can be approached in different ways, of which the most important can be the study of the clustering of galaxies and the bound systems defined by their spatial distribution, and the statistical measures of the properties of galaxies and how these vary with their environment.

There have been several attempts to characterise galaxy properties as a function of local density (Bromley et al., 1998; Garilli et al., 2001; Ramella et al., 1998; Croton et al., 2005). In particular, studies of the variation of the luminosity function include the luminosity function of wall and void galaxies in the 2dFGRS (Croton et al., 2005), in the SDSS (Hoyle et al., 2004), and theoretical variations in the lumi-

nosity function as a function of local galaxy density (Mo et al., 2004).

In this paper we concentrate on the study of the variations of the luminosity function with local density, which we characterise by the distance to the nearest group of galaxies, normalised by the group radius. We approach this problem by first studying numerical simulations with semi-analytic galaxies, to later corroborate with mock 2dFGRS catalogues the possibility of applying the method to the real 2dFGRS galaxies, thus providing a new test of the semi-analytic model of galaxy formation.

It should be noted that according to the present understanding of the galaxy formation process, galaxies form exclusively in dark-matter haloes (Kauffmann et al., 1999; Cole et al., 2000; Somerville et al., 2001; Nagashima et al., 2002). Therefore, our analysis does not refer to groups as any

arXiv:astro-ph/0508220v1 9 Aug 2005

dark matter halo, but instead to associations of at least two galaxies with $B_J < -16.5$. This, according to recent measurements of the halo occupation number statistics (Abazajian et al., 2004, in SDSS), can only be found in haloes with $M > 10^{11} M_\odot$. Other studies (Lemson & Kauffmann, 1999) shows a dependence of the halo mass function on the environment. Since the properties of the semi-analytic galaxies depend only on their host halo mass (*), we can also expect a dependence of the luminosity function on the local environment.

This paper is organised as follows. We start by describing the numerical simulation and semi-analytic galaxies used in this work in Section 2, where we also describe the selection of haloes used to characterise the local galaxy density in the simulation box. In Section 3 we describe the method and algorithms used to determine the luminosity function corresponding to the different semi-analytic galaxy environments. We present the results from the numerical simulation galaxies in Section 4, and study the possibility of detecting such results in the 2dFGRS by applying the method to mock 2dFGRS catalogues in Section 5. In Section 6 we show the results from the real 2dFGRS catalogue, and finally in Section 7 we conclude our work with a summary of our main conclusions.

2 THE NUMERICAL SIMULATION

The numerical simulation used in this work, kindly provided by the Cosmology group at Durham group, comprises data on dark matter particles and on GALFORM semi-analytic galaxies. The numerical simulation box is $250h^{-1}\text{Mpc}$ a side, and contains 125,000,000 particles. The process by which the distribution of dark matter particles was populated by galaxies can be found in Cole et al. (2000), and can be summarised as follows. After haloes of at least 10 dark matter particles are identified in the simulation using a Friends-of-friends algorithm, the GALFORM algorithm produces a Monte-Carlo merger history for each halo which defines the galaxies that populate it. We emphasize that the properties of these galaxies depend only on the halo mass, and not on the environment in which each halo resides. These galaxies are characterised by magnitudes in several bands (of which we only make use of the B_J band), and stellar formation rate parameters, plus spatial positions and peculiar velocities. The total number of galaxies in the simulation box is approximately 1.8 million. Due to the dynamical limitations of the numerical simulation, the galaxy sample is limited by an absolute magnitude limit of $B_J < -16.5$.

* The only input to the semi-analytic model coming from the numerical simulation is the halo mass. Therefore, any influence from large scale (i.e. the environment external to the halo in the simulation) has no direct influence on the resulting semi-analytic galaxies. On the other hand, the physics implemented by the semi-analytic model can have a much more noticeable impact on the properties of semi-analytic galaxies; in this work, the physics governing the evolution of galaxies is held fixed and correspond to the Benson et al. (2003) model.

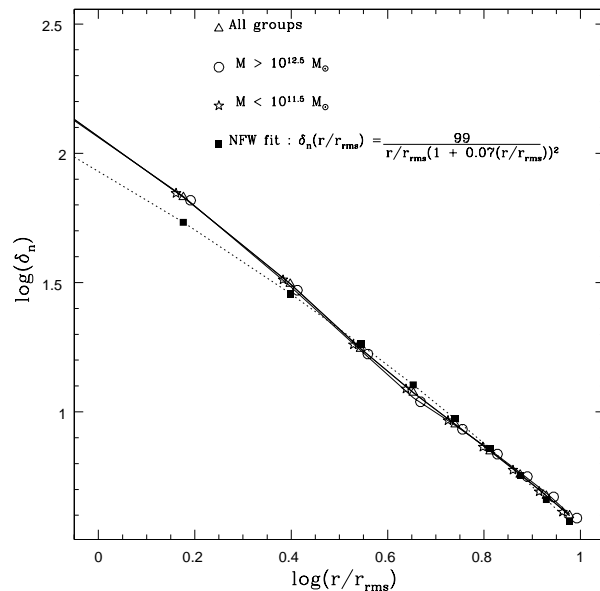


Figure 1. Comparison between the density profiles of galaxies and mass around haloes in the numerical simulation cube.

3 METHOD

In this paper we characterise the density at which a galaxy resides by locating the dark-matter halo that is closest to the galaxy position in units of halo/group radius, denoted by r_{rms} , calculated as half the mean projected distance between pairs of galaxies in a group. We use a normalised distance (r/r_{rms}) in order to take into account the different halo sizes. This is motivated by the clear indications from numerical simulations that the galaxy density around dark-matter haloes depends on the normalised distance and on the halo concentration parameter (Navarro, Frenk & White, 1996, NFW). Figure 1 shows the density profile around haloes for the dark-matter (dotted line) using NFW profile, and for galaxies in halos with different mass ranges in the simulation (solid lines). The galaxy density profile shows no important variation with the halo mass. As can be seen, even though the halo concentrations vary between the different samples of haloes shown in the figure, there is little difference between the dark-matter and galaxy density profiles, even for $\log(r/r_{rms}) < 0.3$, the dark-matter density is only lower than the galaxy density by about a factor of 0.9. This fundamental result supports our hypothesis that a sample of galaxies lying within a given range of normalised distances to halo centres are characterised by the same local galaxy or dark-matter density.

The procedure to define our semi-analytic galaxy subsamples can be described as follows: 1. Calculate the distance from each galaxy to the nearest haloes. 2. Assign this galaxy to the halo that presents the shortest normalised distance r/r_{rms} to the galaxy. 3. Divide the galaxy sample according to the normalised distance to the closest halo. This process produces galaxy subsamples that are characterised by a complicated spatial distribution which is depicted in Figure 2 from different viewpoints (Top left: Front view, Top right: Side-view, Lower panels, angle views); in this ex-

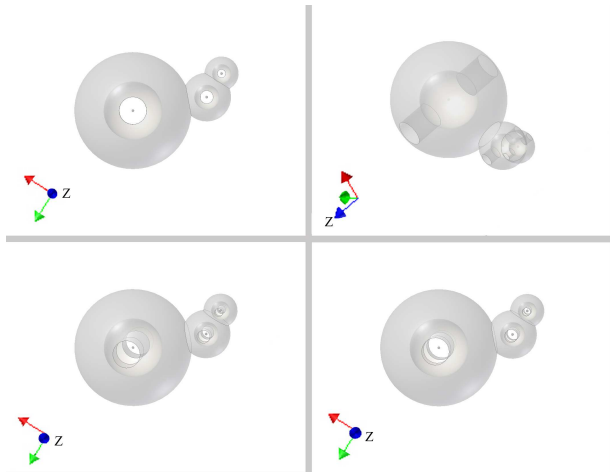


Figure 2. Schematic representation of the geometry of the problem. The subsample of galaxies selected according to $1 < r/r_{rms} < 2$ fills the spherical volumes depicted in this figure. The cylindrical volumes are oriented in the direction of the line of sight (z -axis), and are removed from our analysis when effects of peculiar velocities need to be avoided.

ample we have three shells of equal density for three groups of galaxies (each sphere corresponds to a different group).

As we are interested in assessing the possibility of applying this method to real data, the different observational biases present in real data samples have to be taken into account as well. One of the effects that will prove particularly important for our work is that of peculiar velocities in redshift surveys, which causes the well known finger-of-god effect around groups and clusters of galaxies. This effect makes a galaxy that is sitting in the middle of the cluster potential well appear spuriously far away from the cluster centre. This will lead us to induce that this galaxy belongs to a subsample characterised by a low density environment due to its spuriously large separation from the halo centre and will introduce a systematic error in our measurements. In order to avoid this problem, we simply remove a cylinder centered on the halo centre and aligned with the direction of the line of sight. In the case of the simulation box, we take this direction to be the z -axis. Note that in Figure 2 we have removed these cylinders from the spheres surrounding each group.

The galaxy subsample selection criteria and the removal of a cylinder shaped volume to avoid the effects of peculiar velocities makes it difficult to estimate the normalization of the luminosity function. Therefore, in cases when an estimate of the volume is needed we also produce a catalogue of random positions which populate the same regions occupied by the galaxy subsample of interest. Such random catalogues are produced using the same halo centres in the numerical simulation and following the steps used for defining the galaxy subsamples, but this time using the random particles instead of semi-analytic galaxies.

The luminosity functions (LF hereafter) are calculated using the standard STY (Sandage, Tammann & Yahill,

1979), Step Wise Maximum Likelihood (SWML, Efsthathiou, Ellis, & Peterson, 1988) and $1/V_{MAX}$ (VMAX, Schmidt, 1968, Huchra & Sargent, 1973) methods. As Willmer (1997) provides a detailed review on the three different methods, we only present their most relevant characteristics. The VMAX method is the most popular of the three, and weights each galaxy by the volume corresponding to the maximum distance out to which it would remain below the magnitude limit of the survey. This method also provides the normalization of the LF, but it does not take into account the fact that galaxies present a clustered distribution. Another setback of the VMAX method is that it requires the counts of galaxies to be binned in magnitude, which makes data of individual galaxies to be lost. The STY method is a maximum likelihood estimator, which has the advantage of calculating a likelihood for each individual galaxy, as well as being an unbiased estimator of the LF for a clustered spatial distribution of galaxies. One drawback is that this method does not provide the normalization of the LF and assumes a fixed functional form for the shape of the LF, usually a Schechter function (Schechter, 1976). The SWML method is similar to the STY method, in that it is also a maximum likelihood method, but it does not assume a specific shape of the LF since it uses galaxies binned in consecutive absolute magnitude intervals. In the case of the STY and SWML methods, the normalization is calculated using the estimators given by (Davis & Huchra, 1982).

We will quantify the luminosity function by quoting the values of the parameters M^* and α in the Schechter formula:

$$\phi(M)dM = 0.4 A \ln 10 \phi^* e^{-X} X^{\alpha+1} dM,$$

where $X = 10^{0.4(M^* - M)}$, and the parameter M^* refers to the characteristic luminosity of the sample of galaxies; α is the faint-end slope and indicates the relative importance of a population of low luminosity galaxies. For instance, a large, negative value of $\alpha = -1.7$ indicates a large population of dwarf galaxies; ϕ^* is the normalization of the LF which we choose not to calculate since this parameter traces the density profile around groups of galaxies or dark-matter haloes.

4 NUMERICAL SIMULATION RESULTS

The mass function of haloes in the numerical simulation is well described by the Jenkins et al. (2001) formula, which is characterised by a large population of low mass haloes, and a few, rare, high mass objects with $M > 10^{15} M_{\odot}$. Observational catalogues face little difficulties in detecting the high mass objects, but cannot observe galaxies fainter than the apparent magnitude of the survey, which translates into an approximate lower mass cut-off in the catalogue. For example, in the 2dFGRS Percolation Inferred Galaxy Group catalogue (2PIGG), this is $M_{low} \simeq 10^{11} M_{\odot}$ (Eke et al. 2004).

In order to illustrate what would be found in the dependence of the luminosity function with normalised distance to the halo centres, we first select from the simulation, haloes with a distribution of masses resembling that of an observational sample of groups. In particular, we use the distribution of masses in the full 2PIGG presented by Eke et al. (2004). In Figure 3 we show the distribution of masses in the simulation and in a 2dFGRS mock catalogue. We then

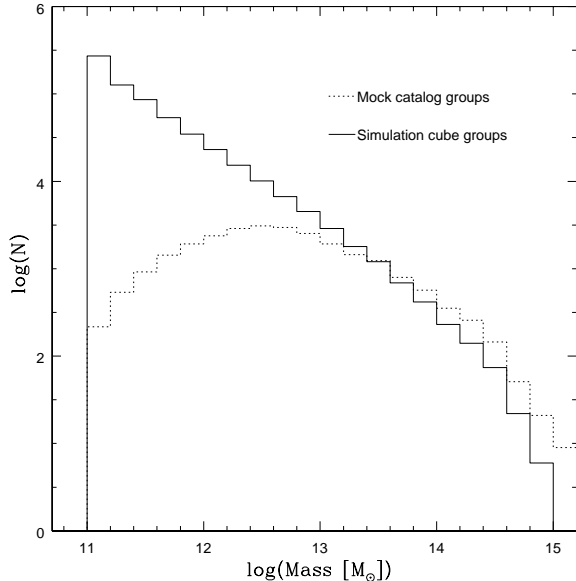


Figure 3. Selection of haloes from the numerical simulation box so as to match the mass distribution of the mock catalogue.

select haloes from the simulation so that they show the same distribution of masses as the 2PIGG. As can be seen, this is very similar to placing a lower limit on the halo mass of $M > 10^{11} M_{\odot}$.

It should be noted that as the semi-analytic model for galaxy formation only takes into account the mass of the dark matter halo when populating it with galaxies, the dependence of the luminosity function with normalised distance responds to variations in the mass function of low mass haloes around larger dark-matter haloes (in order to improve clarity, we will refer to the latter as simulated clusters). Figure 4 shows the variations in halo mass function as the normalised distance (r/r_{rms}) to a nearby simulated cluster increases. The differences in amplitude respond mainly to the variation in density around simulated clusters; for instance, in the cluster central regions, the density is about 2 orders of magnitude larger than the mean in the simulation, thus explaining the 2 order of magnitude difference between the dotted and solid lines. In this Figure there is a striking lack of high mass haloes in the mass function of haloes in the simulated cluster outer regions compared to the inner haloes at $r/r_{group} < 2$; this is caused by the selection of clusters in the simulation, which contains all the high mass haloes with masses $M > 10^{13} h^{-1} M_{\odot}$. The resulting mass functions show larger abundances of high mass haloes in the cluster centres, a slight decrease in high mass haloes for the intermediate distances, and again an increase for the larger distances from the simulated cluster centres. On the low mass end of the mass function, it can be seen that the inner haloes present the largest population, whereas this diminishes as we go towards haloes in regions further away from the cluster centres.

Variations in the mass function of low mass haloes around simulated clusters may be biased in the sense that simulations show that the radial distribution of sub-haloes

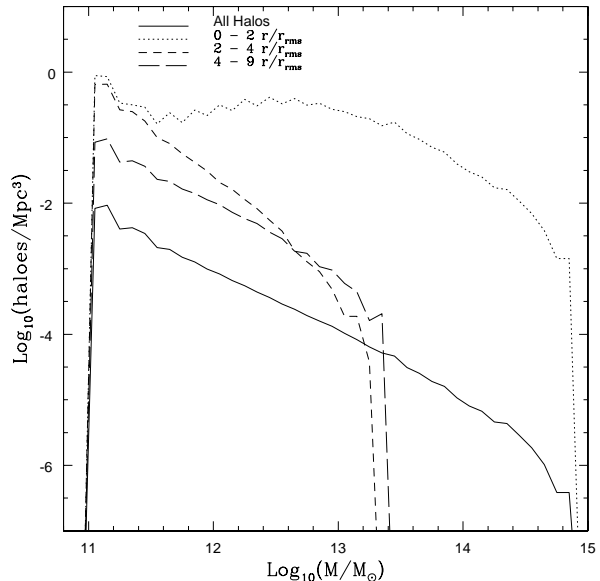


Figure 4. Mass function of haloes at different distances from “centre haloes” (see text). Distance ranges are shown in the key.

within their parent haloes is substantially less centrally concentrated than that of the dark matter (Gao et al., 2004; Nagai et al., 2005). This is not a setback to our procedures since we only argue that the normalised distance between haloes and clusters provides a reasonable proxy for local density. Furthermore, we have shown that semi-analytic galaxies trace the same density profile regardless of the mass of the central cluster.

Given that the properties of semi-analytic galaxies depend only on its host halo mass, the variations in the mass function of haloes on normalised distance to simulated clusters will imprint variations in the LF. For instance, the haloes in the outermost regions contain larger abundance at $M \simeq 10^{13} M_{\odot}$ which contributes satellites galaxies which may increase the value of α . The higher upper limit in halo mass will also induce a change in M^* since larger haloes tend to host the brightest galaxies.

In order to study the variations of the LF in the simulation, we proceed to rank the semi-analytic galaxies according to their normalised distance to the closest halo centre, and produce several subsamples at $0 < r/r_{rms} < 1$, $1 < r/r_{rms} < 2$, and so forth. In a first instance, we use the real-space galaxy positions. Later on, we apply redshift-space distortions by displacing the galaxy z -coordinate positions by an amount equal to the z -component of their peculiar velocities (in units of $h^{-1} \text{Mpc}$).

The results in real-space are displayed in solid lines in Figure 5, where the top panel shows the dependence of M^* on r/r_{rms} , and the bottom panel, the dependence of the parameter α . Error bars correspond to $1-\sigma$ errors calculated using the Jackknife method. All errors in this work are calculated using this method, a choice that is supported by numerous works reporting that Jackknife errors are comparable to the dispersion of results from large numbers of realistic mock catalogues (See for instance, Padilla et al., 2005). As

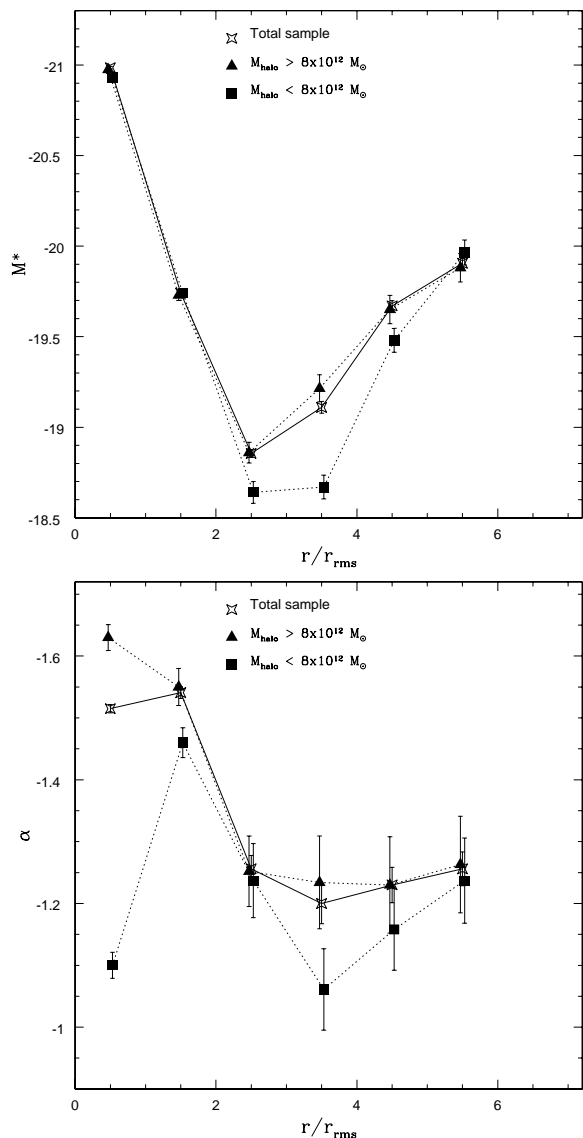


Figure 5. Top panel: Variation of the characteristic absolute magnitude M^* parameter as a function of normalised distance to the group center. Different lines correspond to different ranges in simulated cluster masses (indicated in the key). Bottom panel: Same as top panel but for the faint-end slope of the LF α .

can be seen, the dependence of M^* indicates a population of very bright galaxies near the simulated cluster centres, which dims significantly as we approach a normalised distance of $r/r_{rms} \approx 3$. Interestingly, at $r/r_{rms} \approx 5$, the characteristic luminosity increases to reach a constant value of $M^* = -20$, which is consistent with the value of M^* characterising the full sample of semi-analytic galaxies in the simulation. This in perfect agreement with what was found for the mass function of haloes in the same normalised distance ranges.

Qualitatively, a very similar behaviour can be seen for the parameter α , which is very negative at the centre of the groups, indicating a large population of low luminous galaxies or semi-analytic satellites (low and high mass haloes respectively). At $r/r_{rms} \approx 3$, α reaches its highest value (or

flattest slope) $\alpha \approx -1$, and settles at $\alpha \approx -1.25$ at larger normalised separations. The full sample of galaxies in the simulation shows $\alpha = -1.37$; therefore the galaxies at large separations from groups show a comparable M^* to the full sample of galaxies, but a comparatively low population of dwarf galaxies.

These findings encode a wealth of information regarding the galaxy formation process and possible further evolution. Even though the semi-analytic model for galaxy formation is a relatively simple one, in the sense that it only requires the mass of a host halo in order to populate it with galaxies, it manages to produce answers that can be reconciled with several physical processes that affect the evolution of galaxies. For instance, the dependence of the parameters M^* and α can be understood as follows.

The high luminosity galaxies in the centres of groups along with a large population of dwarfs is a reasonably well documented fact observed in redshift surveys (Blanton et al., 2004) and individual clusters (González et al., 2005; Valotto et al., 2004), and is thought to be a consequence of subsequent mergers of haloes. This preferentially takes place in the centres of groups and clusters of galaxies (massive haloes), where the galaxy density is high. The large population of dwarf galaxies is thought to be produced by the close interaction of haloes, tidal stripping (Mayer et al., 2001) or other processes considered in the semi-analytic model. Note that since this simulation only takes into account dark-matter interactions, no gas processes are taken into account.

A new interesting result that can be appreciated in Figure 5 is how extended is the influence of simulated clusters over their surrounding medium. As can be seen, the population of low luminosity galaxies (i.e. low mass haloes) is slightly reduced at distances $r/r_{rms} \approx 3$ (faint M^* and flat α) with respect to the field population, marking the radius of influence of clusters. The mechanisms that produce such effects take place in the cluster centres, so this loss of galaxies may be the consequence of galaxy/halo passages through the near centres of clusters. There is also a clear depletion of low luminosity galaxies (low absolute values of α), which can also be understood in terms of passages of low mass haloes (dwarfs) through the group centres of which a fraction is cannibalised by larger haloes.

Finally, at separations $r/r_{rms} \approx 6$, the behaviour of both M^* and α tends to constant luminosity function parameters for larger separations. Notice that the values of the field LF parameters in the simulation depend on input values that have not been tuned to reproduce exact LF parameters of 2dFGRS data.

We also check whether the variations in luminosity function depend on the mass of the nearby simulated clusters. Figure 5 shows in solid squares and triangles, the resulting variations in M^* and α with r/r_{rms} when the mass of the centre haloes varies (solid squares for low mass haloes, solid triangles for high mass haloes). As can be seen, the characteristic luminosity does not change significantly in the central or more external regions, being the values of M^* consistent when taking as centres either low, high or all the haloes selected. The major difference can be seen at intermediate distances, $r/r_{rms} \approx 3$, where low mass haloes are surrounded by lower luminosity galaxies than higher mass haloes (by almost half a magnitude). Regarding the distance at which M^* tends to a roughly constant value, it can be

argued that lower mass haloes influence a larger volume in terms of their radius, r_{rms} , since M^* remains at low luminosity values out to $r/r_{rms} \simeq 3.5$. The variation in the luminosity function slope α shows that at intermediate distances, low mass haloes contain less low luminosity galaxy neighbours than high mass haloes. On the other hand, at low $r/r_{rms} < 1.5$, the population of faint galaxies decreases dramatically in low mass haloes. In this case the low mass halo sample contains objects with $M < 8 \times 10^{12} h^{-1} M_{\odot}$, which for the magnitude limit of the semi-analytic galaxies in this simulation, corresponds to haloes that preferentially contain 2 or less galaxies, whereas large mass haloes contain large amounts of satellite galaxies which account for this difference.

5 TESTING THE APPLICABILITY OF THE METHOD TO OBSERVATIONAL DATA

As a first check, we repeat the study performed in the previous Section to the full simulation box data, but taking the galaxy positions in redshift-space. In this case, as can be seen in figure 6 shown by the crosses, the effect of peculiar velocities smears the relation seen in the cube in real-space, to a degree that makes it difficult to arrive at any conclusions regarding a dependence of the luminosity function parameters on normalised distance. This is produced by the high velocity dispersions that characterise the centres of galaxy groups and clusters, which produce the finger-of-god effect in redshift surveys, and that spuriously displaces galaxies corresponding to the centres of groups to the group outer regions, thus contaminating the relation between M^* and α with r/r_{rms} . This is a very important effect that needs to be taken into account when analysing redshift space data.

In order to correct for this effect, we proceed to remove from our analysis all those galaxies that lie within a cylindrical volume centred on the group centres and aligned with the direction over which the galaxy positions were displaced by their peculiar velocities (the z-axis in this case). We experiment with different cylinder radii and show different symbols in Figure 6 (see the key). As can be seen, this technique is able to partially recover the qualitative shape of the dependence of both M^* and α with r/r_{rms} found using the full simulation box in real-space. Notice that as we increase the cylinder radii to reduce the peculiar velocity effect, we lose data of central galaxies in groups, so we test with different cylinder radii. We select an optimal value for this parameter such that it minimises the effects from redshift-space distortions and low-number statistics, $r_c = 0.5r_{rms}$. This is the value of r_c that we will adopt from now in the analysis of both mock and real catalogues, unless otherwise stated.

5.1 The 2dFGRS galaxy and group catalogues

Before going any further, we describe the characteristics of the observational data. The 2dFGRS survey (Colless et al., 2001, & 2003) comprises a total of $\sim 230,000$ low resolution spectra of galaxies distributed in two regions near the North and South galactic poles (NGP and SGP regions respectively) covering a total of about 2000 deg^2 on the sky. The apparent magnitude limit of the survey is of the order of $b_J < 19.4$ with plate-to-plate variations on the sky of about

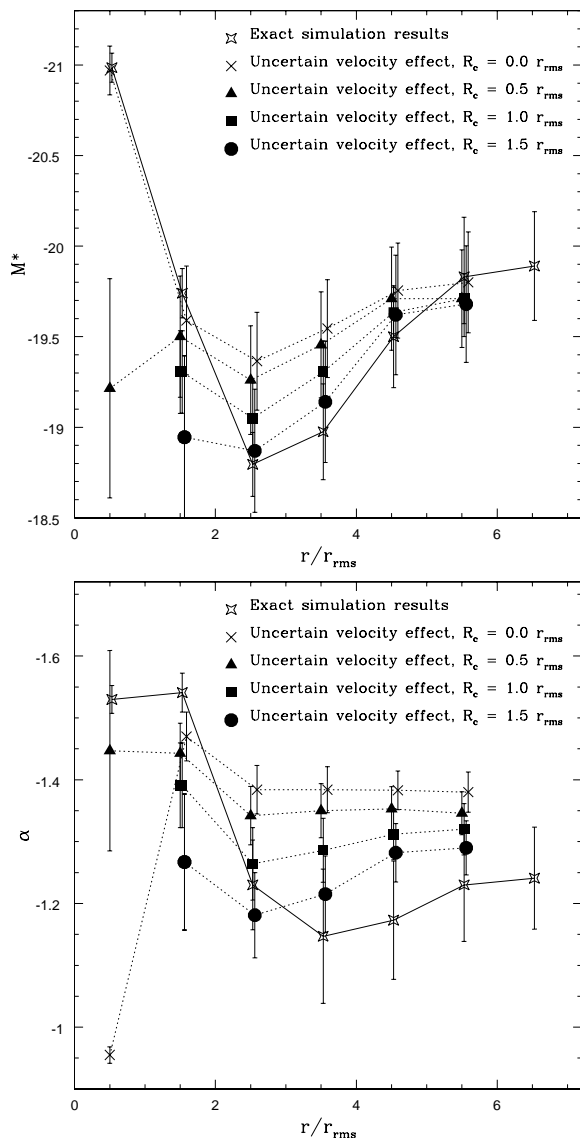


Figure 6. Top panel: Variation of the characteristic absolute magnitude M^* as a function of normalised distance to the group center. Different symbols correspond to different radii for the cylindrical volume that is removed from the analysis in order to avoid contamination of the clusters inner galaxies on outer shells due to the velocity dispersion of the clusters. Bottom panel: Same as top panel but for the faint-end slope, α .

0.2 magnitudes. The parent imaging 2dFGRS catalogue is the Automated Plate Machine survey, APM (Maddox et al., 1990). The survey presents a complicated angular completeness mask which has also been made available by the 2dFGRS Team and which we use in all of our following analyses. When measuring luminosity functions using 2dFGRS data, we pay special attention to remove angular incompleteness effects by weighting each galaxy by the inverse of the incompleteness factor at its position (this information is part of the public 2dFGRS data). This incompleteness factor includes effects from fiber collisions, and therefore our results are expected to be free from such effects.

The galaxy groups to be used in our analysis are taken from the 2PIGG catalogue (Eke et al., 2004), which contains groups of galaxies identified in the 2dFGRS with at least 2 members. There is a total of 30,000 groups in the 2PIGG catalogue. The advantage in using this particular sample of groups relies in the careful calibration of the friends-of-friends (FOF) method in Eke et al. (2004) using detailed mock 2dFGRS catalogues. The distribution of group r_{rms} radii show only a few hundred groups with $r_{rms} < 30$ arcseconds, with a typical $r_{rms} = 4$ arcminutes. This indicates that there is little effect on our results from this problem, which we also correct for by applying a completeness weight. At any rate, our conclusions from the 2dFGRS are only relevant at distances $r > 2r_{rms}$ from the group centres; a study of the group central regions would need a more careful treatment of this problem.

We will now test whether we can use the 2dFGRS groups and galaxies to detect the variations in the LF of Section 4 using mock catalogues.

5.2 Mock 2dFGRS galaxy and group catalogues

We use the semi-analytic galaxies in the numerical simulation to produce mock 2dFGRS and 2PIGG catalogues. We place an observer at a random position in the simulation box, then simulate the observing biases including variable magnitude limits, angular incompleteness masks, and $(k+e)(z)$ corrections from Norberg et al. (2002). The final mock 2dFGRS catalogue contains comparable numbers of members in the NGP and SGP areas.

We then feed the mock 2dFGRS catalogue into the FOF algorithm kindly provided by Vincent Eke, and produce a mock 2PIGG catalogue. One of the advantages of the mock 2PIGG catalogue over the real 2PIGG is that we also know the true mass of each galaxy group. The true mass of a group is that of the halo in the numerical simulation box corresponding to the galaxy group in the mock catalogue.

Therefore, these mock catalogues match as closely as possible the properties of the observational dataset, and will make it possible for us to assess whether the properties of the luminosity function of galaxies at different normalised distances from galaxy groups can be measured with the real 2dFGRS dataset.

5.3 Application to mock catalogues

The first check we perform on the mock catalogues is that we actually recover the Schechter function parameters of the underlying luminosity function in the numerical simulation. Figure 7 shows the likelihood contours on the $\alpha - M^*$ plane that correspond to the 1- (solid lines), and 2- σ (dotted lines) levels, using different methods for estimating the luminosity function. The large empty circle represents the simulation underlying luminosity function, and as can be seen, the SWML method provides the most accurate answer from the mock NGP region.

After checking that we can recover the galaxy luminosity function within at least 2- σ of the underlying values, we proceed to rank galaxies according to their minimum normalised distance to galaxy groups, just as we did with the semi-analytic galaxies in the simulation box (in the real and

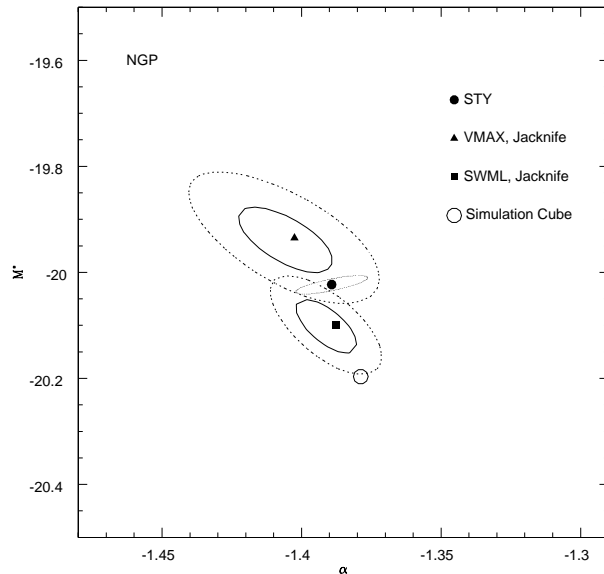


Figure 7. Contour plots for the best fit luminosity function parameters found from the mock catalogue, compared to the underlying simulation value. Solid lines: 1- σ contours. Dotted lines: 2- σ contours.

mock catalogues we actually use the projected positions of group member galaxies to estimate the group radius, r_{rms}). The resulting luminosity function parameters can be seen in Figure 8, for for a cylindrical volume of radius $r_c = 0.5r_{rms}$, that is removed from the analysis in order to avoid the finger-of-god effects. For comparison, this Figure also shows the results from the full numerical simulation box in real-space. As expected, it is difficult to recover exactly the behaviour for α and M^* seen in the simulation box. Moreover, there is no apparent trend in the Schechter parameters with r/r_{rms} , except for a marginal signature of a minimum in the α parameter at $3 r/r_{rms}$, which is in agreement with the simulation box results.

Still, it is extremely important that the results are not seriously affected by spurious variations of M^* and α , incompatible with the simulation box results. Therefore, any features in M^* and α seen in the observational data will likely correspond to actual underlying changes in these parameters.

6 2DFGRS RESULTS

We start this Section by corroborating that our algorithm provides reliable measurements of the LF by first calculating the 2dFGRS LF using the full sample of galaxies and comparing it to previous measurements. Applying the SWML algorithm we find the Schechter parameter combination $\alpha = -1.26 \pm 0.03$, $M^* = -19.84 \pm 0.11$, and $\phi^* = 0.0159 \pm 0.0030$. These results are in agreement ($\simeq 1\text{-}\sigma$) with measurements of the B_J galaxy luminosity function from the ESO Slice Project by Zucca et al. (1997), who find $\alpha = 1.22 \pm 0.07$, $M^* = -19.61 \pm 0.08$ and $\phi^* = 0.020 \pm 0.004$; and a measurement of the 2dFGRS galaxy luminosity func-

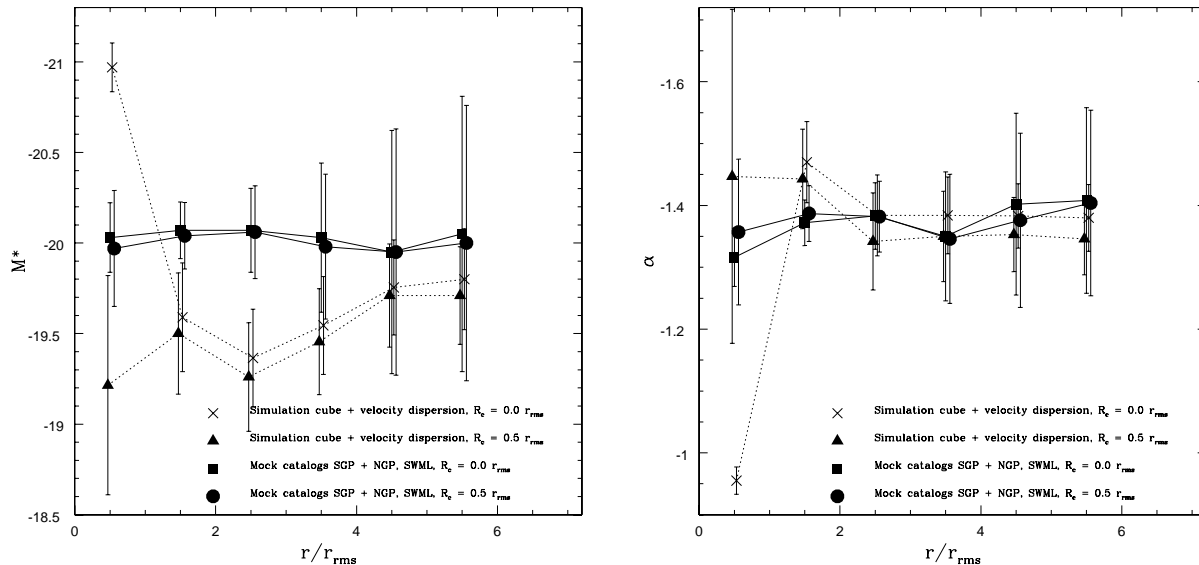


Figure 8. Left panel: Variation of the characteristic absolute magnitude, M^* as a function of normalised distance to the group center in the mock catalogues (solid lines). For comparison, results from the full simulation box are also shown (dotted lines). Different symbols correspond to different choices of cylinder radii removed to avoid contamination of group inner galaxies on the outer shells, due to the galaxy velocity dispersion in groups. Right panel: Same as top panel but for the α parameter.

tion by Norberg et al. (2002), who obtain $\alpha = 1.21 \pm 0.02$, $M^* = -19.66 \pm 0.06$ and $\phi^* = 0.0161 \pm 0.0005$. It should be noted that we do not intend to provide a new measurement of the galaxy luminosity function in the 2dFGRS, this is only to demonstrate that the code used in this work provides reasonable answers.

The reader should bear in mind that the semi-analytic model is an approach that aims to reproduce the outcome of many real processes involved in the formation of galaxies, and that this result is tied to a particular cosmological model. Therefore, on a direct comparison between mocks and real data, several characteristics of the numerical and semi-analytical models should be taken into account (For instance, differences in the strength of the peculiar velocity field between mock and real data can produce different responses to the method when using real data). Therefore, the actual variations of the Schechter parameters as a function of r/r_{rms} may be completely different to what we found in the semi-analytic simulation. We bear these possible differences in mind and proceed to apply the method to the real 2dFGRS and 2PIGG catalogues following the same steps from the previous Section.

After ranking the 2dFGRS galaxies by r/r_{rms} we measure the luminosity functions and present the Schechter parameters α and M^* in Figure 9. In this figure, the left panels show the dependence with normalised distance, and the right panels the dependence on $1+\delta$, which assuming a NFW profile around the 2PIGG galaxy groups, corresponds to the dark matter density in terms of the mean density.

Results from the NGP region are similar to those from the mock catalogues in that there is no clear trend in the Schechter parameters with r/r_{rms} given the error bars. However, the SGP region shows a dip in both, M^* and α at the expected $r/r_{rms} = 3$. At $r/r_{rms} \simeq 6$ the Schechter parameters converge to values marginally consistent with the

field luminosity function parameters (Norberg et al., 2002; de Lapparent et al., 2003).

This result is very encouraging and may be interpreted as a possible, new success of the semi-analytic galaxy formation model. The implications for this are dramatic since only one parameter, namely the mass of a dark-matter halo can reproduce an intuitive life cycle for a galaxy/halo in the nearby regions of clusters, including passages, cannibalism, and stripping of dark-matter from tidal encounters. Still, the reader should be reminded that this is only a marginal detection on the SGP region of the 2DFGRS.

The right panels of Figure 9 show the dependence of the Schechter parameters on density contrast $1 + \delta$. When analysing these results it should be kept in mind that the density contrast quoted in these panels corresponds to that of a NFW profile centred on the galaxy groups. Were this profile a fair representation of the dark-matter density profile of real galaxy groups, then our values of $1 + \delta$ would correspond to the actual dark-matter density in which our samples of galaxies are embedded. These results are compatible and complementary to those from Mo et al. (2004), who study the changes in M^* and α in the range $-1 < \log(1 + \delta) < 1$. There is a clear overlap between our results and Mo et al. at $\log(1 + \delta) = 1$, and we extend this measurement to $\log(1 + \delta) = 2.5$.

We perform a final analysis of the luminosity function around groups. This time we take the full 2dFGRS catalogue and divide our sub-samples of galaxies at different r/r_{rms} by the luminosity of the nearest galaxy group at $L = 10^{10.5} L_{\odot}$. Figure 10 shows the results, and indicates that the luminosity function of galaxies around the brighter groups contain an excess of dwarf galaxies when compared to fainter groups, at least for $r/r_{rms} > 1$, as indicated by the more negative values of the parameter α . Also, as expected, the typical luminosity of objects in brighter groups

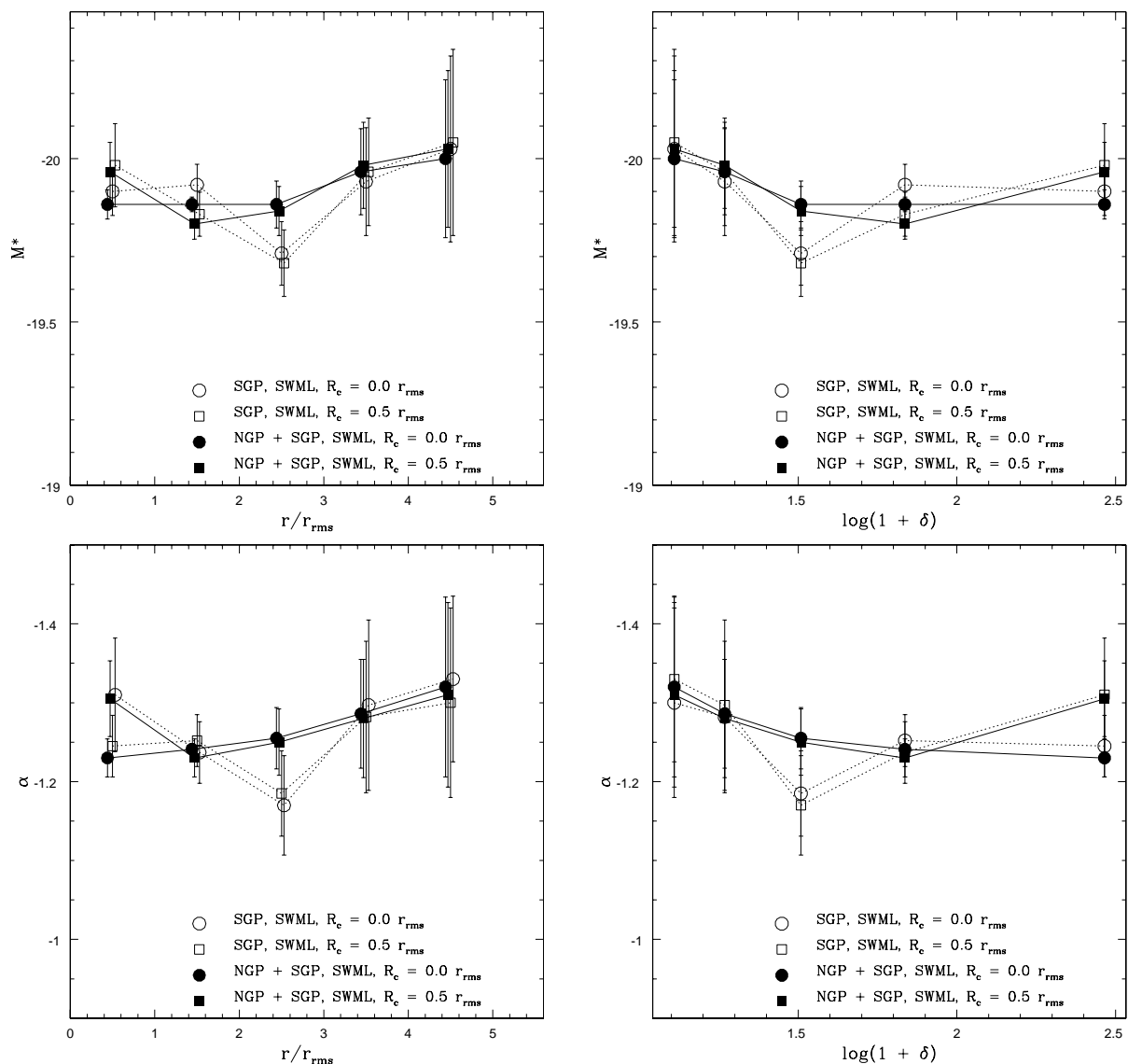


Figure 9. Top panels show the variation of the characteristic absolute magnitude, M^* as a function of normalised distance to the group center (left panels) and dark matter density (right panels) in the 2dFGRS. Different lines correspond to different cylinder radii to avoid contamination of group inner galaxies on outer shells due to the velocity dispersion of the groups. Bottom panels are the same as top panels but for the LF faint-end slope, α .

is higher than in fainter groups, as indicated by the more negative values of M^* in bright groups. In this case, this effect is seen at all values of r/r_{rms} . If we compare the LF for different halo masses in Figure 5 with the luminosity dependence in Figure 10 we can see that brighter groups behave similarly than massive haloes except for the inner regions $r/r_{rms} < 2$ where the results in both figures do not match; However, at $r/r_{rms} \simeq 3$ we can see the dip of α and M^* at larger normalised distance for low mass haloes or less luminous haloes. It has been shown that the total luminosity of a group is an excellent tracer of group mass (Eke et al. 2004, Padilla et al. 2004), as our results also show. This Figure also shows a marginal detection of a more extended dip in M^* for the low Luminous clusters, although it would be necessary to study a larger sample of groups and galaxies

than the 2dFGRS dataset to be able to measure the upturn in M^* at larger separations.

7 CONCLUSIONS

We presented a study on the variations of the luminosity function of galaxies around clusters of galaxies in numerical simulations with semi-analytic galaxies. The aim of this work was to quantify the extent of the influence of clusters on their environments and to assess whether such effects can be reproduced by a semi-analytic model where the main parameter determining the population of galaxies are the halo masses.

In order to do this, we select a population of haloes from

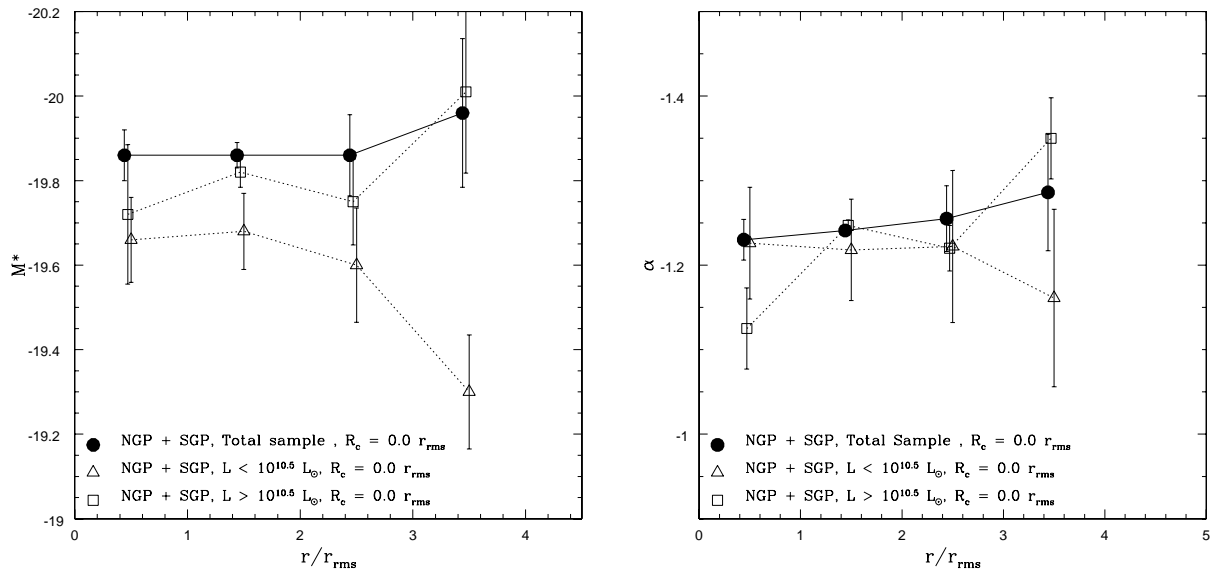


Figure 10. Left panel: Variation of the characteristic absolute magnitude, M^* as a function of normalised distance to the group center in the 2dFGRS. Different lines correspond to different galaxy luminosities. Right panel: Same as top panel but for the α parameter.

the numerical simulation which are set to be the clusters of our simulation. These are characterised by the same distribution of mass found for the groups in a mock 2PIGG catalogue. Therefore, the variations we find in the semi-analytic model can be considered as predictions which we also test in this work by applying the method to the 2dFGRS galaxies and 2PIGG groups.

As mentioned above, the main parameter taken into account by the semi-analytic model when producing galaxies is the mass of the halo. Therefore, the variations in the LF parameters M^* and α correspond to variations in the mass function of haloes at different ranges in r/r_{rms} , and when we measure the variations in the luminosity function we are actually measuring changes in the mass function with r/r_{rms} . A good agreement between the variations in the simulated and observed LFs indicates that the mass of a halo correlates very well with the different processes a galaxy may have been subject to during its life.

The semi-analytic galaxy luminosity function shows important variations with the distance to the centres of clusters in the simulation box. We find that galaxies are brighter in the cluster inner regions, and that they show a minimum in characteristic luminosity at intermediate distances, $r/r_{rms} \simeq 3$. At larger separations, the characteristic luminosity increases and tends to a constant value, $M^* \simeq -20$. The minimum in M^* is interpreted as a measure of the zone of influence of clusters in terms of their radius. We also find a similar behaviour in α , which indicates a massive abundance of low luminosity galaxies (low mass haloes and/or semi-analytic satellites) in the cluster central regions, which decreases to a minimum at intermediate distances, and increases again at $r/r_{rms} \simeq 5$ to reach a constant value, somewhat lower in absolute value than for the full semi-analytic galaxies.

We interpret these results as clusters being capable of cannibalising small haloes from nearby regions out to 3 virial

radii from their centre, and also of stripping the mass of normal haloes. These two effects would explain the high luminosity central galaxies surrounded by numerous low luminosity satellites. The former can be the result of successive mergers of haloes, whereas the latter can be thought of as captured low mass haloes from nearby regions, and relatively high mass haloes from nearby regions which have been tidally stripped off part of their mass. This would also explain the lack of high and low luminosity semi-analytic galaxies from the region around $r/r_{rms} \simeq 3$.

By properly taking into account observational biases, we checked whether the variations found in the luminosity function of galaxies around groups in the simulation box can be measured using available data from redshift surveys. First we study the effect that the velocity dispersion of galaxies in groups induces in our results when the galaxy positions are measured in redshift space. When no corrections for this effect are attempted, we find that the dependence of the Schechter parameters is almost completely erased. One way to avoid this is the removal of cylinders centred on each group, aligned with the line of sight. The most convenient value for the projected radius of the cylinder is about $r_c = 0.5r_{rms}$.

Once we demonstrate that it is possible to find variations in the luminosity function from redshift data (at least qualitatively), we test whether this can still be detected using the 2dFGRS galaxies and 2PIGG groups, which are available to the astronomical community. The 2dFGRS is affected by a series of observational biases such as a complicated incompleteness mask and radial selection function, which can make it even more difficult to detect the variations in the luminosity function. Therefore, we produce mock catalogues which reproduce as closely as possible all the observational biases present in the real data. When we do this, we find that the dependence of the Schechter parameter on the normalised distance to group centres is almost completely

lost. This indicates that the removal of a cylindrical volume around groups is not enough to recover the underlying variations in the luminosity function, but that the measurements do not return spurious answers either.

When applying the method to real data, we find that the luminosity function of galaxies in the 2dFGRS NGP strip shows no variations in M^* or α with the normalised distance to the group centres. However, we do find a minimum value in M^* and α in the luminosity function of the SGP region, in agreement with our results from the semi-analytic model. Further agreement between the data and the semi-analytic model is found in the correlation between the luminosity of galaxies and that of their neighbour galaxy group, which is seen in the simulation as a correlation between halo mass and the luminosity of the surrounding galaxies. Also, the data is marginally consistent with a dip in M^* for the low luminosity 2PIGG groups, again in agreement with the results from the full simulation box. These results strongly indicate that the interpretation given to the simulation results could actually have taken place in the formation history of 2dFGRS galaxies.

We have shown in this work that the variation of the galaxy luminosity function around groups and clusters of galaxies is a powerful tool for understanding the processes that galaxies are subject to in the vicinities of clusters. It is left to forthcoming efforts to assess whether the variations in the LF are also accompanied by changes, for instance, in the surface brightness of galaxies, as this galaxy property is also believed to be influenced by the presence of a nearby cluster or group of galaxies (or by its absence, as in a low surface brightness galaxy). This as well as other galaxy properties can be studied to complement the results obtained in this work. A future application of the method presented here that would benefit from improved statistics is the study of the regions surrounding groups in the Sloan Digital Sky Survey (Abazajian et al. 2004), which in the very near future will double the number of galaxies available in the 2dFGRS. This method can also be applied to deep, wide area surveys (such as the GALEX medium spectroscopic survey, Morrissey et al. 2005) which will make it possible to detect variations of galaxy properties around groups with redshift providing a study of the evolution of the influence of clusters on their surrounding environments throughout the history of the Universe.

ACKNOWLEDGMENTS

This work was supported in part by the DAA-ESO grant at PUC, NDP was supported by a Proyecto Postdoctoral Fondecyt no. 3040038, GG is supported by Proyecto Regular Fondecyt no. 1040359. RG was partially supported by Proyecto Regular Fondecyt no. 1040359. We acknowledge support from the FONDAP Center for Astrophysics. We have benefited from helpful discussions with D. G. Lambas. We thank the Referee for helpful comments and suggestions.

REFERENCES

Abadi, M., Moore, B. & Bower, R., 1999, MNRAS, 308, 947
 Abazajian, K., Zheng, Z., Zehavi, I. et al., 2004, ApJ submitted, (astro-ph/0408003)

Benson, A., Bower, R., Frenk, C., Lacey, C., Baugh, C., & Cole, S., 2003, ApJ, 599, 38.
 Bromley B. C., Press W. H., Lin H., Kirshner R. P., 1998, ApJ, 505, 25
 Blanton, M.R., Lupton, R., Schlegel, D. et al., 2004, ApJ, submitted, (astro-ph/0410164)
 Cole, S., Lacey, C., Baugh, C., & Frenk, C., 2000, MNRAS, 319, 168
 Colless, M., Dalton, G., Maddox, S. et al. (the 2dFGRS Team), 2001, MNRAS, 328, 1039
 Colless, M., Peterson, B., Jackson, C. et al (the 2dFGRS Team), 2003, (astro-ph/0306581)
 Croton, D.J., Glennys, R.F, Norberg, P. et al., 2005, MNRAS, 356, 1155C
 Dalton, G., Efstathiou, G., Maddox, S., Sutherland, W., 1994, MNRAS, 269, 151
 Davis, M., & Huchra, J., 1982, ApJ, 254, 437
 Efstathiou, G., Ellis, R.S., & Peterson, B.A., 1988, MNRAS, 232, 431 (SWML).
 Eke, V. R. et al. (the 2dFGRS Team), 2004, MNRAS, 348, 866
 Garilli, B., Maccagni, D., Stefano, A. et al., 2001, A&A, 342, 408
 Gao, L., White, S., Jenkins, A. et al., 2004, MNRAS, 255, 819G
 González, R. E., Lares, M., Lambas, D. G., & Valotto, C., 2005, A&A submitted
 Hoyle F. & Vogeley, M.S., 2004, ApJ, 607, 751
 Huchra, J.P., & Sargent, W.L.W., 1973, ApJ, 186, 433.
 Jenkins, A., Frenk, C. S., White, S. et al. 2001, MNRAS, 321, 372
 Kauffmann, G., 1999, AAS, 31, 1470
 Kundic, T., Spergel, D. & Hernquist, L., 1993, AAS, 25, 1428
 de Lapparent, V., Galaz, G., Bardelli, S. & Arnouts, S. 2003, A&A, 404, 831
 Lemson, G., Kauffman, G., 1999, MNRAS, 302, 111
 Maddox, S., Efstathiou, G., Sutherland, W., & Loveday, J., 1990, MNRAS, 243, 692
 Mayer, L., Governato, F., Colpi, M., et al., 2001, ApJ, 559, 754
 Mo, H.J, Yang, X., van den Bosh, F.C., Jing, Y. P., 2004, MNRAS, 349, 205
 Moore B., Lake, G., Quinn, T., & Stadel, J., 1999, MNRAS, 304, 465
 Morrissey, P., et al. (the GALEX Team), 2005, ApJ, 619, L7.
 Nagai, D. & Kravtsov, A., 2005, ApJ, 618, 557N
 Nagashima, M., Yoshii, Y., Totani, T., & Gouda, N., 2002, ApJ, 578, 675
 Navarro, J. F., Frenk, C. S., & White, S. D. M., 1996, ApJ, 462, 563 (NFW)
 Navarro, J. F., Frenk, C. S., & White, S. D. M., 1997, ApJ, 490, 493 (NFW)
 Norberg, P. et al. (the 2dFGRS Team), 2002, MNRAS, 336, 907
 Padilla, N., Infante, L., Flores, S., Asséf, R., Gawiser, E., & Christlein, D., 2005, submitted to MNRAS.
 Padilla, N., Baugh, C., Eke, V. et al. 2004, MNRAS, 352, 211
 Ramella, M., Zamorani, G., Zucca, E., 1998, A&A, 342, 1
 Sandage A., Tammann G.A., & Yahill, A. 1979, ApJ 232, 352 (STY).
 Schechter, P., 1976, APJ, 203, 297
 Schmidt, M., 1968, ApJ, 151, 393.
 Somerville, R., Lemson, S., Sigad, Y. et al. 2001, MNRAS, 320, 289
 Valotto, C., Muriel, H., Moore, B. & Lambas, D., 2004, ApJ, 603,67
 Willmer, C.N.A., 1997, AJ, 114, 898